$LiAlO_2$ Modified Li Negative Electrode with $Li_{10}GeP_2S_{12}$ Electrolyte for Stable All-Solid-State Lithium Batteries

Xinshuang Chang [a,c], Wei Weng [a], Mengqi Li [a], Ming Wu [a], George Z. Chen [f], Kam Loon Fow [c,d,e], Xiayin Yao [a,b*]*

[a] *Ningbo Institute of Materials Technology and Engineering, Chinese Academy of Sciences, Ningbo 315201, P.R. China*

[b] *Center of Materials Science and Optoelectronics Engineering, University of Chinese Academy of Sciences, Beijing 100049, P. R. China*

[c] *Department of Chemical and Environmental Engineering, Faculty of Science and Engineering, University of Nottingham Ningbo China, Ningbo 315100, P.R. China*

[d] *Key Laboratory of Carbonaceous Wastes Processing and Process Intensification of Zhejiang Province, University of Nottingham Ningbo China, Ningbo 315100, P.R. China*

[e] *Nottingham Ningbo China Beacons of Excellence Research and Innovation Institute, University of Nottingham Ningbo China, Ningbo, China*

[f] *Department of Chemical and Environmental Engineering, Faculty of Engineering, University of Nottingham, University Park, Nottingham NG7 2RD, UK*

** Corresponding Authors: kam-loon.fow@nottingham.edu.cn; yaoxy@nimte.ac.cn*

ABSTRACT

Lithium (Li) metal has an ultrahigh specific capacity in theory with an extremely negative potential (versus hydrogen), receiving extensive attentions as the negative electrode material in batteries. However, formation of Li dendrites and unstable interfaces due to the direct Li metal reaction with solid sulfide-based electrolytes is hindering the application of lithium metal in all-solid-state batteries. In this work, we report the successful fabrication of $LiAlO_2$ interfacial layer on the Li/$Li_{10}GeP_2S_{12}$ interface through magnetic sputtering. As $LiAlO_2$ can be a good Li^+ ion conductor but an electronic insulator, the $LiAlO_2$ interface layer can effectively suppress Li dendrite growth and the severe interface reaction between Li and $Li_{10}GeP_2S_{12}$. The Li@$LiAlO_2$ 200nm/$Li_{10}GeP_2S_{12}$/Li@$LiAlO_2$ 200nm symmetric cell can remain stable for 3000 h at 0.1 mA cm^{-2} under 0.1 mAh cm^{-2}. Moreover, unlike the rapid capacity decay of the cell with pristine lithium negative electrode, the Li@$LiAlO_2$ 200nm/$Li_{10}GeP_2S_{12}$/$LiCoO_2$@$LiNbO_3$ cell delivers a reversible capacity of 118 mAh g^{-1} and a high energy efficiency of 96.6% after 50 cycles. Even at 1.0 C, the cell with the Li@$LiAlO_2$ 200nm electrode can retain 95% of the initial capacity after 800 cycles.

KEYWORDS: $LiAlO_2$, interface modification, lithium negative electrode, $Li_{10}GeP_2S_{12}$, magnetic sputtering, all-solid-state batteries

1. INTRODUCTION

Lithium-ion batteries (LIBs) are manufactured for various purposes, particularly consumer electronic devices.[1-3] Nevertheless, all commercial LIBs cannot yet reach the

high energy density needed for larger scale energy storage.[4, 5] In part, this is due to the capacity of graphite negative electrode approaching its theoretical limit (372 mAh g^{-1}).[6, 7] Lithium metal wins over many others as an ideal negative electrode with 0.534 g cm^{-3} in density, 3860 mAh g^{-1} in specific capacity, and −3.04 V in potential (*vs* standard hydrogen electrode).[8-10]

However, lithium dendrites growth and detrimental interface side reactions have seriously limited the using of lithium metal negative electrode.[11] Inorganic solid electrolytes of high mechanical strength are promising candidates for preventing the penetration of lithium dendrites.[12] Among those studied inorganic solid electrolytes, $Li_{10}GeP_2S_{12}$ is widely recognized to be highly conductive to Li ions and capable of effective dendrites suppression.[13, 14] Thus, all-solid-state lithium metal batteries (ASSLMB) with solid electrolyte are developed to offer greatly enhanced energy capacity surpassing that of currently available LIBs.[15, 16] Lithium metal, unfortunately, can reduce $Li_{10}GeP_2S_{12}$ easily to various products (Li-Ge alloy, Li_2S, Li_3P) of high electron conductivity. These continuously formed reduction products accumulate at the interface, leading to a large increase of the cell impedance and rapid cell failure.[17]

So far, constructing a protective layer is a viable strategy to strengthen the $Li_{10}GeP_2S_{12}$/lithium metal interface. For example, research have demonstrated the improved interface stability by introducing Li_3PO_4,[18] LiF,[19] and BN [20] layer at the $Li_{10}GeP_2S_{12}$/lithium metal interface. In addition, alloys such as Li-Ag,[21] Li-Mg [22] have also been used as a buffer layer to provide effective protection for $Li_{10}GeP_2S_{12}$. All the artificial layers mentioned above can physically isolate the electrolyte and lithium

metal, preventing $Li_{10}GeP_2S_{12}$ from being reduced by lithium metal. However, lithium dendrites are still growing during the cycle, and lithium alloy interface layers are not reversible, which cannot meet the application requirements of ASSLMB. Therefore, it is urgent to find a stable coating with good ion conductivity which can effectively hinder the reduction of $Li_{10}GeP_2S_{12}$ by lithium metal but also block the growth of lithium dendrites. It has been reported that Li-containing compounds coatings with good Li-ion conductivity could induce good electrochemical performance for LIBs. As $LiAlO_2$ phase can facilitate the hopping of lithium ions in the boundary region, it possesses good ability to conduct lithium ions.[23, 24] Zhang et al. has demonstrated that $LiAlO_2$ coated on $Na_2Li_2Ti_6O_{14}$ could provide fast charge transmission paths for lithium ions in LIBs.[25] Thus, we envision that a $LiAlO_2$ coating can also be used to guard the deposition of lithium metal at the interface between lithium and $Li_{10}GeP_2S_{12}$ in ASSLMB.

For use in ASSLMB, the $LiAlO_2$ protection layer must be fabricated with the thinnest possible thickness so that the diffusion of Li ions is not completely obstructed while the Li dendrite formation is adequately hindered. However, to the best of our knowledge, there is no report of investigation of the performance of $LiAlO_2$ layer on $Li/Li_{10}GeP_2S_{12}$ interface for ASSLMB. Therefore, there is a need to develop a suitable methodology for fabrication of $LiAlO_2$ thin film with an optimally thin thickness at the $Li_{10}GeP_2S_{12}$/lithium metal interface of ASSLMB. Due to its insulating behavior, $LiAlO_2$ thin film is usually grown on Li metal substrate *via* chemical deposition methods, such as atomic layer deposition [26] and chemical vapor deposition [27], or

physical deposition methods, such as magnetic sputtering [28]. Amongst these deposition methods, magnetron sputtering offers a wider range of advantages, such as simpler instrumentation, no constraint of substrate morphology and induce no reaction with the substrate surface.[29, 30]

In this work, we first report an ease to reproduce methodology for deposition of thin insulating layer of $LiAlO_2$ for use in ASSLMB via magnetron sputtering. Specifically, the $LiAlO_2$ interface layer was constructed on lithium surface through the radio frequency magnetic sputtering method which can fabricate uniform and dense coatings to provide effective protection for $Li_{10}GeP_2S_{12}$. The $LiAlO_2$ layer is capable of physically isolating lithium metal from $Li_{10}GeP_2S_{12}$. In addition, the decomposition of $Li_{10}GeP_2S_{12}$ resulting from reduction by lithium metal can be effectively suppressed by the $LiAlO_2$ layer, thus achieving a greatly improved stability of the $Li_{10}GeP_2S_{12}$/Li interface. More importantly, the $LiAlO_2$ layer with high mechanical property could prevent lithium dendrite growth. Consequently, the Li@$LiAlO_2$ 200nm/$Li_{10}GeP_2S_{12}$/Li@$LiAlO_2$ 200nm symmetric cell remained highly stable as long as 3000 h during the 0.1 mA cm^{-2} cycling test at a capping capacity of 0.1 mAh cm^{-2}. As expected, the cell of Li@$LiAlO_2$ 200nm/$Li_{10}GeP_2S_{12}$/$LiCoO_2$@$LiNbO_3$ revealed a reversible capacity of 78 mAh g^{-1} with 95% in capacity retention after 800 cycles at 1.0 C.

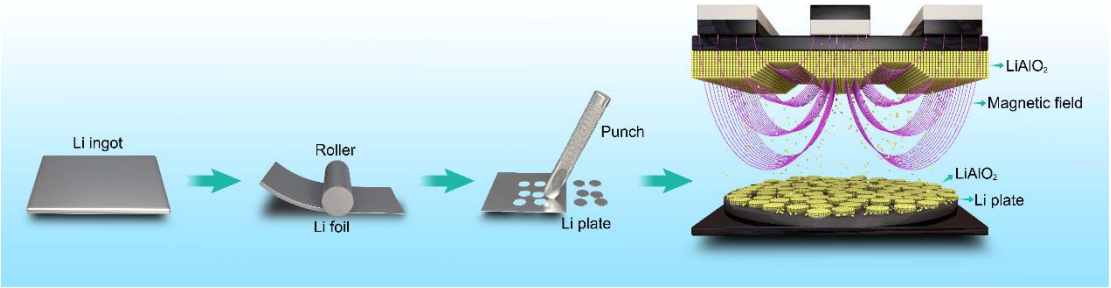

Figure 1. Schematic illustration of preparation procedures of Li@$LiAlO_2$ electrode.

2. EXPERIMENT

2.1 Preparation of Li@$LiAlO_2$ electrode

The target material of $LiAlO_2$ was obtained from Zhongnuo New Materials (Beijing) Technology Co., Ltd. Figure 1 schematically illustrates the preparation procedure for the Li@$LiAlO_2$ electrode. The diameter and thickness of the Li metal plate are 10 mm and 0.5 mm, respectively. The $LiAlO_2$ layer was magnetically sputtered on the lithium plate at a pressure of 0.5 Pa. All samples were fabricated and examined in argon-filled glove boxes. The magnetic sputtering (RH450) apparatus was coupled to a glove box so that the samples were protected by inert gas before and after sputtering. Lithium with $LiAlO_2$ thicknesses of 100 nm, 200 nm and 300 nm are labeled as Li@$LiAlO_2$ 100nm, Li@$LiAlO_2$ 200nm and Li@$LiAlO_2$ 300nm, respectively.

2.2 Characterization of the $LiAlO_2$ Layer

To characterize the Li@$LiAlO_2$ morphology and elemental information, a scanning electron microscope (SEM, Regulus-8230, Hitachi) with energy dispersive X-ray spectroscopy (EDX) analyzer was used. The valence state of elements on the $LiAlO_2$ layer was further confirmed using an AXIS Ultra DLD X-ray photoelectron

spectroscopy (XPS) system. The test data were corrected with the standard value of C-C binding energy, and the CasaXPS software was used for peak fitting. The elastic modulus of the $LiAlO_2$ layer was evaluated on a scanning probe microscope (SPM, Dimension ICON, Bruker).

2.3 Fabrication of symmetric and all-solid-state cells

Lithium symmetrical cells were fabricated by inserting the $Li_{10}GeP_2S_{12}$ electrolyte between two Li@$LiAlO_2$ electrodes. Specifically, 150 mg of $Li_{10}GeP_2S_{12}$ powder were pressurized to form the dense electrolyte layer under 240 MPa. Then two Li@$LiAlO_2$ foils with different $LiAlO_2$ thickness were attached on both sides of the $Li_{10}GeP_2S_{12}$ layer and compressed under 360 MPa. Mixed $LiCoO_2$@$LiNbO_3$ and $Li_{10}GeP_2S_{12}$ with 7:3 weight ratio was used as the positive electrode material for the fabrication of all-solid-state cells. The positive electrode material was uniformly dispersed on $Li_{10}GeP_2S_{12}$ layer and compressed at 120 MPa. Subsequently, on the other side of the $Li_{10}GeP_2S_{12}$ layer, Li@$LiAlO_2$ 200nm or Li as negative electrode was attached and compressed under 360 MPa. For the fabrication of three-electrode cells, Li@$LiAlO_2$ 200nm/$Li_{10}GeP_2S_{12}$/Li@$LiAlO_2$ 200nm and Li/$Li_{10}GeP_2S_{12}$/Li with lithium metal reference electrode were assembled to investigate the separate lithium plating and stripping behavior. All batteries were fixed with screws and nuts and tested without applying additional pressure. The stainless steels were used as current collectors.

2.4 Electrochemical Measurements

The electrochemical performance of Li@$LiAlO_2$ or Li electrode was performed by using a multichannel battery analyzer (LAND CT-2001A). Three-electrode cells were examined by using the electrochemical workstation (1470E, Solartron).

3. RESULTS AND DISCUSSION

As presented in Figure 2a and Figure S1, the surface of pristine lithium metal shows an uneven morphology with evident minor cracks and quickly becomes black after being exposed to air. Whereas the uniform surface morphology of Li@$LiAlO_2$ 200nm and homogeneously distributed Al element (Figure 2b) demonstrate that a dense $LiAlO_2$ layer was successfully fabricated on lithium metal, which guard the lithium from reacting with air (Figure S1). The thickness of $LiAlO_2$ can be characterized by the transversal surface based on the element Al distribution (Figure 2c), which is around 200 nm. Besides, $LiAlO_2$ layers with thickness of 100 nm and 300 nm were also fabricated on the surface of lithium, as shown in Figure S2. XPS was used to characterize the $LiAlO_2$ due to its amorphous nature.[31] Figure 2d shows the XPS results of the $LiAlO_2$ layer. The peak at 530.6 eV is corresponding to the O 1s in the $LiAlO_2$ (Figure 2e), and the peak at 55.1 eV, which is assigned to the Li 1s (Figure 2f) in the $LiAlO_2$ layer, is different than that of lithium metal (55.4 eV). Also, the peak at about 74.8 eV (Figure 2g), which is close to the binding energy of Al^{3+} in $LiAlO_2$ [32], further confirms the existence of $LiAlO_2$ layer. Moreover, the mechanical property of the $LiAlO_2$ layer was investigated by SPM. As shown in Figure 2h, the smooth surface of the $LiAlO_2$ layer indicates a uniform formation of the $LiAlO_2$ coating. The high elastic

modulus (Figure 2i) concentrated between 20-50 GPa (＞10 GPa of the lithium dendrite) [33] is beneficial to prevent the penetration of lithium dendrites [34, 35].

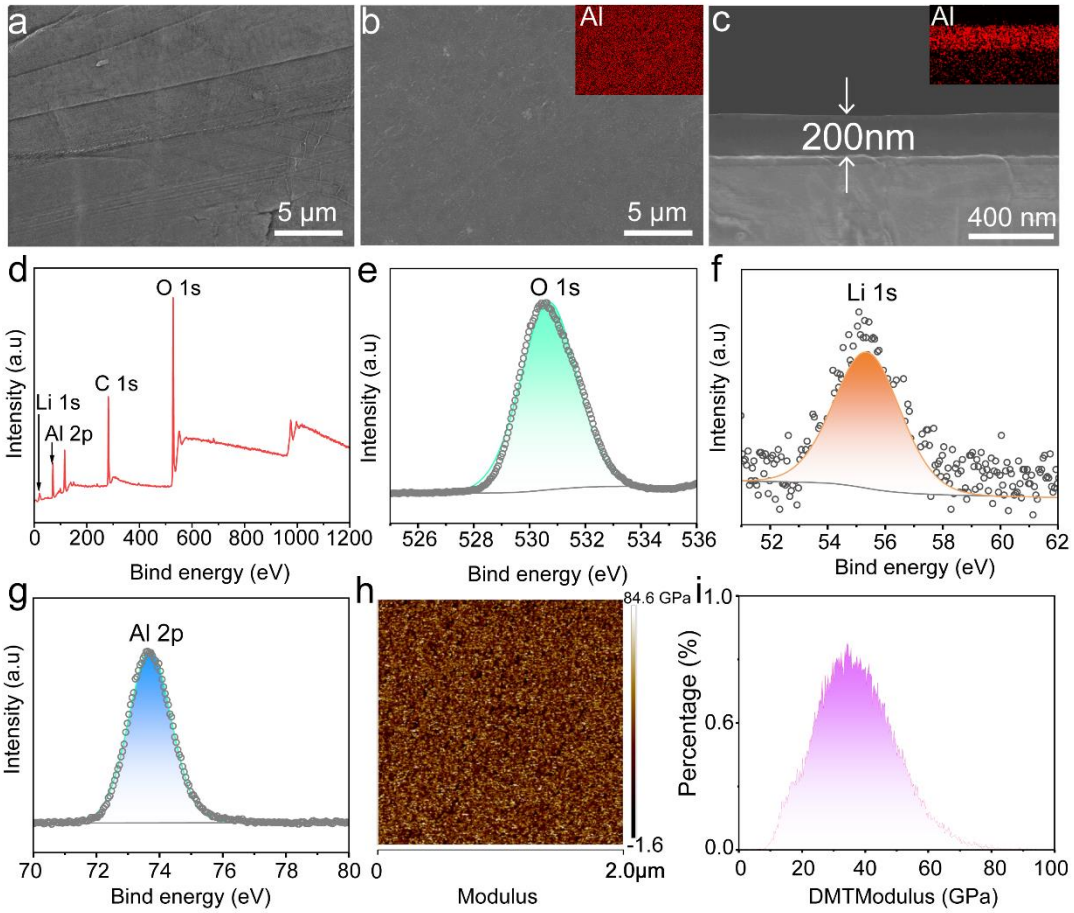

Figure 2. SEM images of (a) Li, (b) Li@$LiAlO_2$ 200nm and (c) sectional view of Si@$LiAlO_2$ 200nm, and the corresponding EDX elemental mapping of Al. XPS spectra of (d) Original XPS survey spectra. High-resolution pattern of (e) O 1s, (f) Li 1s and (g) Al 2p for Li@$LiAlO_2$ 200nm. (h) SPM image and (i) elastic modulus distribution of $LiAlO_2$ layer.

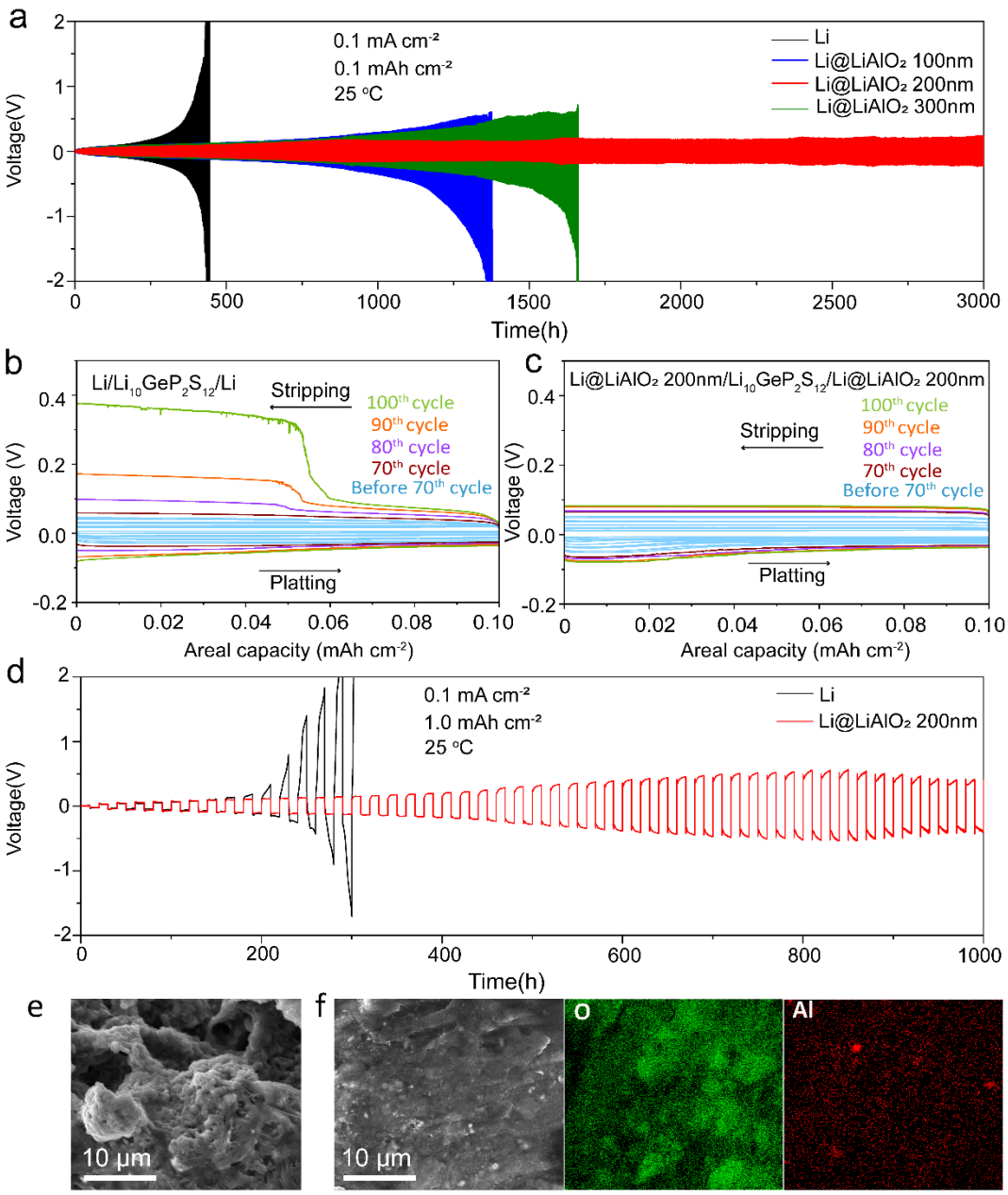

Figure 3. Cyclic stability of symmetric cells with Li@$LiAlO_2$ 100nm, Li@$LiAlO_2$ 200nm, Li@$LiAlO_2$ 300nm and Li at (a) 0.1 mAh cm^{-2}, lithium plating and stripping behavior on (b) lithium/$Li_{10}GeP_2S_{12}$, (c) Li@$LiAlO_2$ 200nm/$Li_{10}GeP_2S_{12}$ interface in three electrodes cells, (d) symmetric cell with Li@$LiAlO_2$ 200nm and Li at 1.0 mAh cm^{-2} and 0.1 mA cm^{-2}. SEM images of (e) Li and (f) Li@$LiAlO_2$ 200nm electrode and corresponding elements distribution of O and Al after deposits of 1 mAh cm^{-2} Li.

To assess the effectiveness of the $LiAlO_2$ on the protection of $Li_{10}GeP_2S_{12}$/lithium, Li@$LiAlO_2$/$Li_{10}GeP_2S_{12}$/Li@$LiAlO_2$ and Li/$Li_{10}GeP_2S_{12}$/Li were assembled and tested at 0.1 mA cm^{-2}. Compared with rapid increase overpotential of Li/$Li_{10}GeP_2S_{12}$/Li, the symmetric cell with Li@$LiAlO_2$ 200nm can stably cycle up to 3000 h at 200 mV and 0.1 mAh cm^{-2} (Figure 3a). However, when the thickness of $LiAlO_2$ decreased to 100 nm, the Li@$LiAlO_2$ 100nm/$Li_{10}GeP_2S_{12}$/Li@$LiAlO_2$ 100nm cell only cycled for 1400 h with a large polarization voltage and then failed quickly, which probably due to the $LiAlO_2$ 100 nm film is too thin to withstand the multiple stripping and plating of lithium metal. While when the thickness of $LiAlO_2$ increased to 300 nm, the symmetric cell with Li@$LiAlO_2$ 300nm can only cycle for 1600 h before its failure. Therefore, compared with Li@$LiAlO_2$ 100nm and Li@$LiAlO_2$ 300nm, the Li@$LiAlO_2$ 200nm electrode possesses the best stability in the lithium platting/stripping process. The separate platting and stripping voltage were explored in the three electrodes cell at 0.1 mAh cm^{-2}. As shown in Figure 3b, an obvious asymmetry in the polarization between stripping and plating was observed for pristine lithium metal. Generally, voids will form in the stripping process and lead to a decrease in the contact area between the Li metal and the solid electrolyte, thus leading to an increase in the local current density and voltage of stripping. However, in the plating process, Li deposition is initiated at the triple point where the Li metal, solid electrolyte, and void meet, and then grow along the free surface of the void. Then many voids will be filled by Li, which will cause a low local current density and polarization, thus resulting in asymmetric voltage of stripping and plating.[36] The platting voltage reached to 100 mV, and the stripping

voltage quickly increased to 380 mV after 100 cycles, showing an uneven contact due to the formation of by-products and dendrites on lithium/$Li_{10}GeP_2S_{12}$ interface. In comparison, the platting and stripping voltage plateaus are quite smooth for the cell with Li@$LiAlO_2$ 200nm electrodes (Figure 3c). The platting voltage is stable at around 78 mV, and the stripping voltage only reached to 80 mV after 100 cycles, indicating an intimate and stable contact between the lithium meatal and $Li_{10}GeP_2S_{12}$ due to the suppressed formation of by-products resulting from the parasite reactions and lithium dendrites under the protection of $LiAlO_2$. With further increased areal capacity of 1.0 mAh cm^{-2} (Figure 3d), Li@$LiAlO_2$ 200nm/$Li_{10}GeP_2S_{12}$/Li@$LiAlO_2$ 200nm can stably cycle up to 1000 h, which is much better than Li/$Li_{10}GeP_2S_{12}$/Li with 300 h. The SEM images of the Li and Li@$LiAlO_2$ 200nm electrodes are also investigated after depositing 1.0 mAh cm^{-2} of lithium, as shown in Figure 3e and f. The surface of Li electrode is uneven and accompanied by lithium dendrites (Figure 3e). By contrast, Li@$LiAlO_2$ 200nm electrode possesses flat and dense surface (Figure 3f), and elements of Al and O are still well distributed, which indicates that the protection layer of $LiAlO_2$ remains relatively intact after lithium platting.

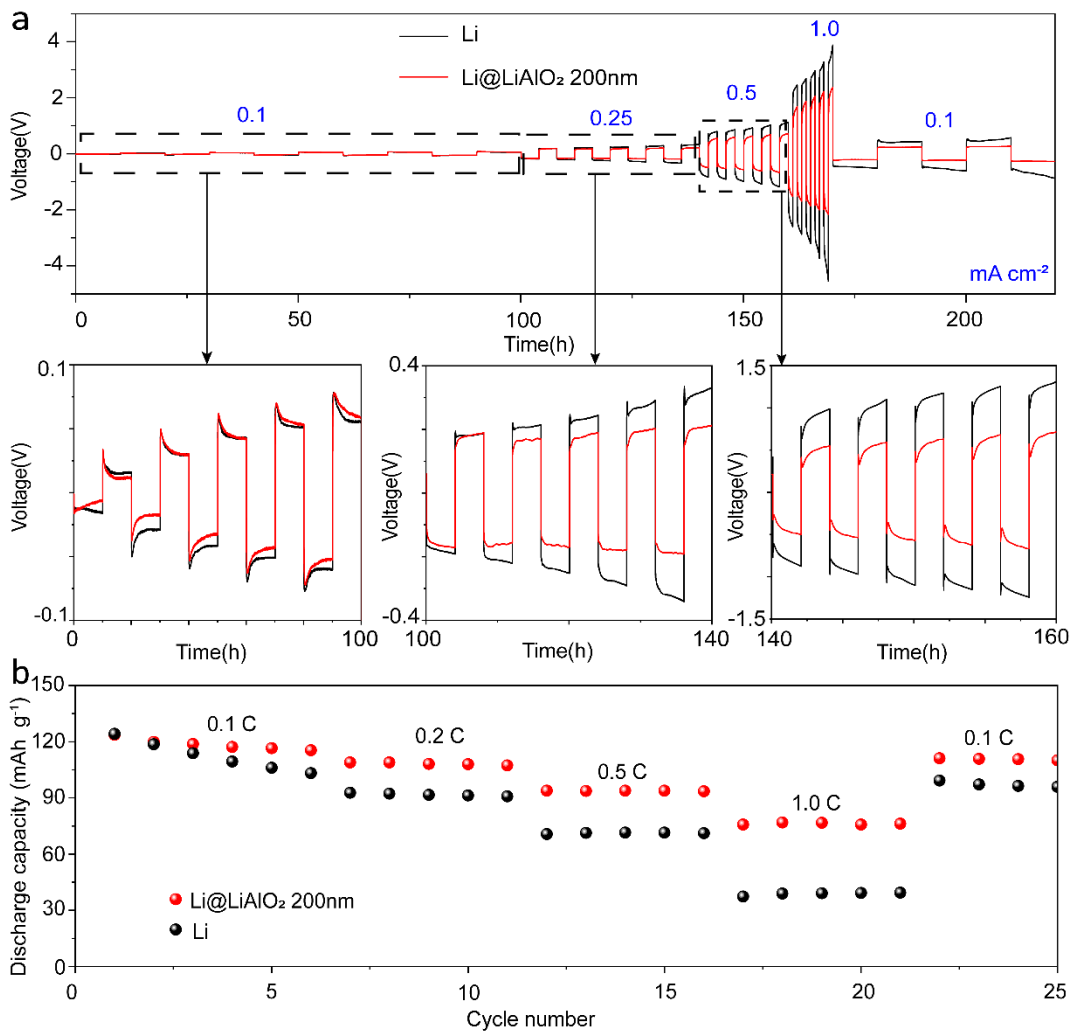

Figure 4. Rate capabilities of (a) Li@$LiAlO_2$ 200nm/$Li_{10}GeP_2S_{12}$/Li@$LiAlO_2$ 200nm and Li/$Li_{10}GeP_2S_{12}$/Li symmetric cells at 0.10, 0.25, 0.50 and 1.00 mA cm^{-2}, respectively. (b) The Li@$LiAlO_2$ 200nm/$Li_{10}GeP_2S_{12}$/$LiCoO_2$@$LiNbO_3$ and Li/$Li_{10}GeP_2S_{12}$/$LiCoO_2$@$LiNbO_3$ cells cycled at 0.1, 0.2, 0.5, 1.0, 0.1 C, respectively.

Figure 4a compares the rate capabilities of Li@$LiAlO_2$ 200nm/$Li_{10}GeP_2S_{12}$/Li@$LiAlO_2$ 200nm and Li/$Li_{10}GeP_2S_{12}$/Li symmetric cells. Compared with the higher overpotentials of Li/$Li_{10}GeP_2S_{12}$/Li cell observed under 0.1, 0.25, 0.5, 1.0 mA cm^{-2}, the overpotentials of symmetric cell with Li@$LiAlO_2$ 200nm were remarkedly lower. Notably, the overpotential of the symmetrical cell with Li@$LiAlO_2$ 200nm increased from 191 to 2134 mV when the current density was

enlarged from 0.25 to 1.00 mA cm^{-2}, which are much lower than that of $Li/Li_{10}GeP_2S_{12}/Li$ with the overpotential from 1050 to 4000 mV. These results demonstrate that the detrimental side reactions and lithium dendrites growth could be effectively reduced by $LiAlO_2$ layer. Figure 4b shows the rate capabilities of $Li@LiAlO_2$ 200nm$/Li_{10}GeP_2S_{12}/LiCoO_2@LiNbO_3$, the reversible capacities are 125, 110, 94 and 78 mAh g^{-1} at 0.1, 0.2, 0.5 and 1.0 C, respectively. After tested at various current densities from 0.1 to 1.0 C, the reversible capacity can recover to 110 mAh g^{-1} when the current density is reset to 0.1 C. On the contrary, the $Li/Li_{10}GeP_2S_{12}/LiCoO_2@LiNbO_3$ cell possesses lower reversible capacities of 124, 92, 70, 40 mAh g^{-1} under the corresponding current densities from 0.1 to 1.0 C, and the capacity only recovers to 96 mAh g^{-1} under 0.1 C. It further proved good reversibility of capacity at a high current density due to the effectively protection of $LiAlO_2$.

The electrochemical performances of ASSLMB with $Li@LiAlO_2$ 200nm as negative electrode were further evaluated. Figure 5a shows the charge and discharge curve of $Li/Li_{10}GeP_2S_{12}/LiCoO_2@LiNbO_3$, showing rapid capacity decay after 10 cycles, and the large polarization voltages leads to a low energy efficiency which is a detriment to the battery electrochemical performance. In comparison, the $Li@LiAlO_2$ 200nm$/Li_{10}GeP_2S_{12}/LiCoO_2@LiNbO_3$ demonstrates good cyclic performance even after 50 cycles with high reversible capacity of 118 mAh g^{-1} and energy efficiency of 96.6% at 0.1 C (Figure 5b and 5c), which is beneficial for its future practical application for ASSLMB. Even at a high current density of 1.0 C (Figure 5d), the cell of $Li@LiAlO_2$ 200nm$/Li_{10}GeP_2S_{12}/LiCoO_2@LiNbO_3$ delivers an impressive specific

capacity of 78 mAh g^{-1} with a high capacity retention of 95% after 800 cycles. The results show that the suppressed formation of lithium dendrites and generation of by-products lead to an excellent electrochemical performance for the cell with Li@$LiAlO_2$ 200nm even at high current density.

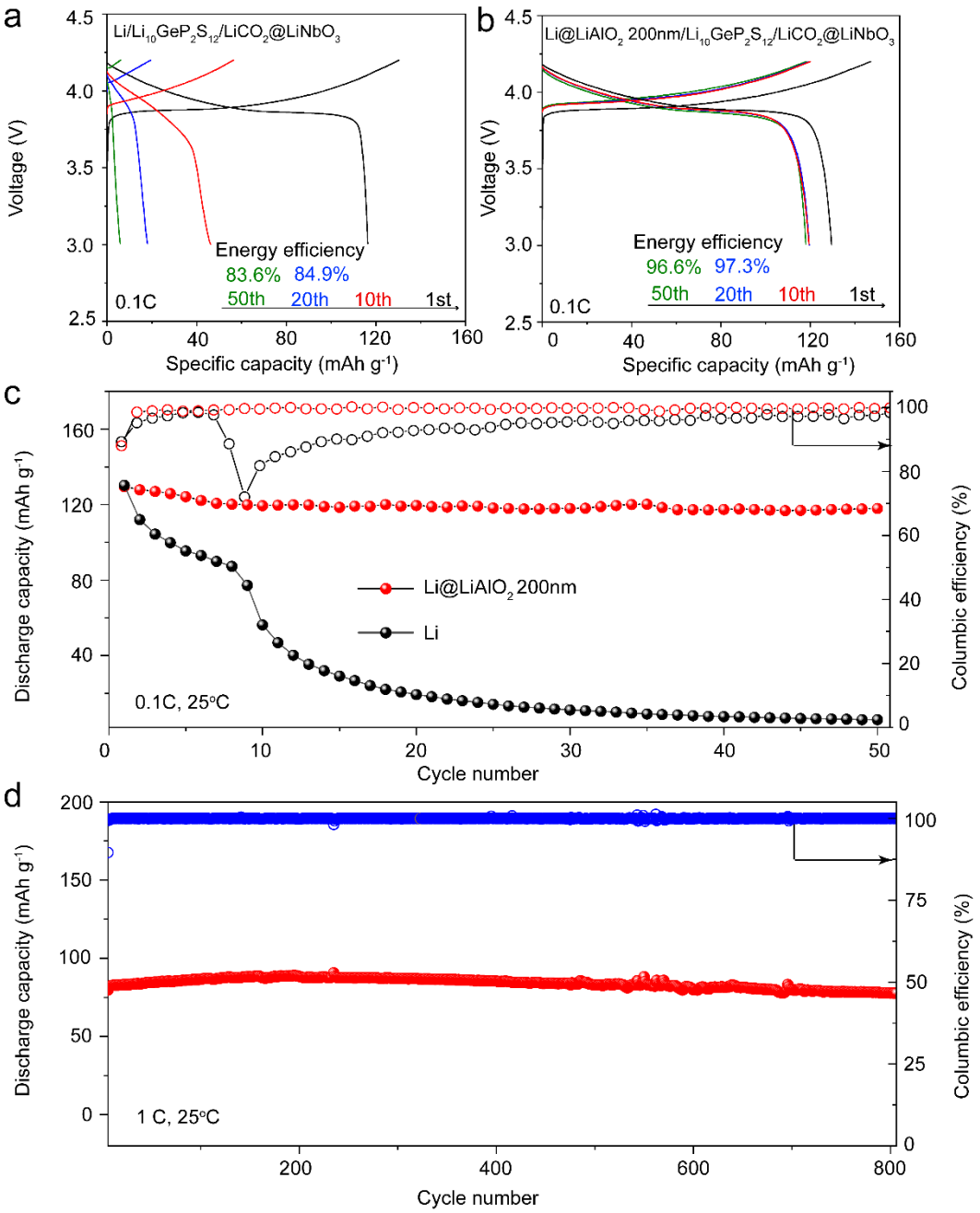

Figure 5. Charge-discharge curves of (a) Li/$Li_{10}GeP_2S_{12}$/$LiCoO_2$@$LiNbO_3$ and (b) Li@$LiAlO_2$ 200nm/$Li_{10}GeP_2S_{12}$/$LiCoO_2$@$LiNbO_3$ cell. (c) Cyclic performances of Li/$Li_{10}GeP_2S_{12}$/$LiCoO_2$@$LiNbO_3$ and Li@$LiAlO_2$

200nm/$Li_{10}GeP_2S_{12}$/$LiCoO_2$@$LiNbO_3$ cell at 0.1 C. (d) Cyclic performances of Li@$LiAlO_2$ 200nm/$Li_{10}GeP_2S_{12}$/$LiCoO_2$@$LiNbO_3$ cell at 1.0 C under 25 ºC.

The performance of the $LiAlO_2$ layer with a thickness of 200 nm is benchmarked against the reported performance of Li_3PO_4, LiF and Li-Ag layers and the performance comparison is shown in Table S1. The cycling stability performance of the $LiAlO_2$ layer is about three times longer than that of the Li_3PO_4, LiF, Li-Ag layers, and the cell with $LiAlO_2$ layer exhibits the highest reversible capacity of 118 mAh g^{-1} after 50 cycles. In addition, the energy efficiency of the cell with $LiAlO_2$ can be maintained at 96.6% at 50^{th} cycle, which is much higher than that of cell with pristine lithium (83.6%). Clearly, the $LiAlO_2$ layer fabricated in this work, which possesses the thinnest thickness and excellent cycle performance, will enable its promising application in the ASSLMB with high energy density in the future.

As illustrated in Figure 6 and Figure S3, the formation of Ge, Li_2S, and Li_3P on the $Li_{10}GeP_2S_{12}$/lithium interface was detected due to the side reactions between the lithium and $Li_{10}GeP_2S_{12}$. In comparison, the $LiAlO_2$ can greatly suppress the formation of by-products while maintaining a good $Li_{10}GeP_2S_{12}$ phase at $Li_{10}GeP_2S_{12}$/Li@$LiAlO_2$ 200nm interface. As shown in Figure S4, the abscissa axis-intercept corresponds to the bulk impedance (R_b) and the semicircle is assigned to the interface impedance of Li/$Li_{10}GeP_2S_{12}$ (R_{ct}), respectively. The R_b and R_{ct} of the cell with Li@$LiAlO_2$ 200nm are 604 Ω and 473 Ω after 50 cycles, respectively. By contrast, pristine Li based cell exhibits much higher values of R_b and R_{ct} with 1399 Ω and 4997 Ω, indicating serious side reactions between the lithium metal and $Li_{10}GeP_2S_{12}$.

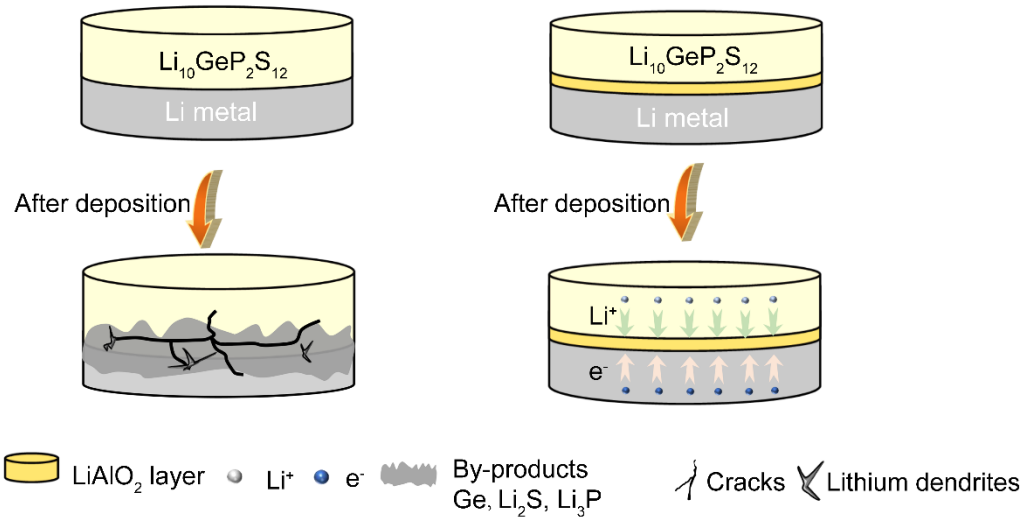

Figure 6. Proposed evolution process on the interface between Li, Li@$LiAlO_2$ 200nm and $Li_{10}GeP_2S_{12}$ after deposition.

4. CONCLUSIONS

A dense and uniform $LiAlO_2$ layer with high mechanic strength was successfully fabricated on lithium metal surface through magnetic sputtering method. The lithium ion conducting but electron insulating $LiAlO_2$ layer could effectively suppress the generation of interface side reactions and lithium dendrites, and greatly improve the stability performance of Li@$LiAlO_2$ negative electrode. By employing the Li@$LiAlO_2$ 200nm in the all-solid state battery, the Li@$LiAlO_2$ 200nm/$Li_{10}GeP_2S_{12}$/Li@$LiAlO_2$ 200nm symmetric cell is able to stably cycle up to 3000 h. The all-solid-state cell with Li@$LiAlO_2$ 200nm shows a high reversible capacity of 78 mAh g^{-1} after 800 cycles at 1.0 C. In addition, the energy efficiency of the cell with $LiAlO_2$ can be maintained at 96.6% after 50th cycle. Obviously, this work presents a method for improving the lithium negative electrode of ASSLMBs based on $Li_{10}GeP_2S_{12}$, and an ideal interface

layer for the preparation of ASSLMB with high energy density in the future.

ASSOCIATED CONTENT

Supporting Information

The following files are available free of charge.

Air stability of Li and Li@$LiAlO_2$, SEM sectional view of Si@$LiAlO_2$ with thickness of 100 nm, 300 nm, XRD patterns of the Li and Li@$LiAlO_2$ 200nm after cycling, EIS of the cells with Li and Li@$LiAlO_2$ 200nm after 50 cycles.

AUTHOR INFORMATION

Corresponding Authors

*Email: kam-loon.fow@nottingham.edu.cn; yaoxy@nimte.ac.cn

ORCID

Xiayin Yao: 0000-0002-2224-4247

Author Contributions

The manuscript was written through contributions of all authors. All authors have given approval to the final version of the manuscript.

Notes

The authors declare no competing financial interest.

ACKNOWLEDGMENT

The work was supported by the National Key R&D Program of China (Grant no. 2022YFB3807700), National Natural Science Foundation of China (Grant no. U1964205, U21A2075, 52172253, 52102326, 52250610214), Zhejiang Provincial Department of Science and Technology (2020E10018), Ningbo Municipal Key Laboratory on Clean Energy Conversion Technologies (2014A22010), Ningbo Natural Science Foundation Programme (Grant No. 2021J186), Jiangsu Provincial S&T Innovation Special Programme for carbon peak and carbon neutrality (Grant No. BE2022007) and Youth Innovation Promotion Association CAS (Y2021080).

REFERENCES

1. Atanu, B.; Asit, T.; Padhy, R. K.; Gautam A. Evaluating the Lithium-Ion Battery Recycling Industry in an Emerging Economy: A Multi-Stakeholder and Multi-Criteria Decision-Making Approach. *J. Clean. Prod.* **2022,** *331*, 130007.

2. Tian, Y.; Lin, C.; Li, H.; Du, J.; Xiong, R. Detecting Undesired Lithium Plating on Anodes for Lithium-Ion Batteries – A Review on the In-Situ Methods. *Appl. Energy* **2021,** *300*, 117386.

3. Manthiram, A., A Reflection on Lithium-Ion Battery Cathode Chemistry. *Nat. Commun.* **2020,** *11* (1), 1550.

4. Zhang, X. G.; Li, Z.; Luo, L. G.; Fan, Y. L.; Du, Z. Y. A Review on Thermal Management of Lithium-Ion Batteries for Electric Vehicles. *Energy* **2021,** *238*, 121652.

5. Xie, J.; Lu, Y. C. A Retrospective on Lithium-Ion Batteries. *Nat. Commun.* **2020,** *11* (1), 2499.

6. Weng, W.; Zhou, D.; Liu, G. Z.; Shen, L.; Li, M. Q.; Chang, X. S.; Yao, X. Y. Air

Exposure Towards Stable Li/$Li_{10}GeP_2S_{12}$ Interface for All-Solid-State Lithium Batteries. *Materials Futures* **2022,** *1* (2), 021001.

7. Masias, A.; Marcicki, J.; Paxton, W. A. Opportunities and Challenges of Lithium Ion Batteries in Automotive Applications. *ACS Energy Lett.* **2021,** *6* (2), 621-630.

8. Li, J. L.; Fleetwood, J.; Blake Hawley, W.; Kays, W. From Materials to Cell: State-of-the-Art and Prospective Technologies for Lithium-Ion Battery Electrode Processing. *Chem. Rev.* **2022,** *122* (1), 903-956.

9. Zhan, R.; Wang, X.; Chen, Z.; Seh, Z. W.; Wang, L.; Sun, Y. Promises and Challenges of the Practical Implementation of Prelithiation in Lithium-Ion Batteries. *Adv. Energy Mater.* **2021,** *11* (35), 2101565.

10. Weiss, M.; Ruess, R.; Kasnatscheew, J.; Levartovsky, Y.; Levy, N. R.; Minnmann, P.; Stolz, L.; Waldmann, T.; Wohlfahrt-Mehrens, M.; Aurbach, D.; Winter, M.; Ein-Eli, Y.; Janek, J. Fast Charging of Lithium-Ion Batteries: A Review of Materials Aspects. *Adv. Energy Mater.* **2021,** *11* (33), 2101126.

11. Zhao, B.; Ma, L.; Wu, K.; Cao, M.; Xu, M.; Zhang, X.; Liu, W.; Chen, J. Asymmetric Double-Layer Composite Electrolyte with Enhanced Ionic Conductivity and Interface Stability for All-Solid-State Lithium Metal Batteries. *Chinese Chem. Lett.* **2021,** *32* (1), 125-131.

12. Wu, J.; Shen, L.; Zhang, Z.; Liu, G.; Wang, Z.; Zhou, D.; Wan, H.; Xu, X.; Yao, X. Y. All-Solid-State Lithium Batteries with Sulfide Electrolytes and Oxide Cathodes. *Electrochem. Energy R.* **2020,** *4* (1), 101-135.

13. Ye, L.; Li, X. A Dynamic Stability Design Strategy for Lithium Metal Solid State

Batteries. *Nature* **2021,** *593* (7858), 218-222.

14. Wang, Y.; Ju, J.; Dong, S.; Yan, Y.; Jiang, F.; Cui, L.; Wang, Q.; Han, X.; Cui, G. Facile Design of Sulfide-Based all Solid-State Lithium Metal Battery: In Situ Polymerization within Self-Supported Porous Argyrodite Skeleton. *Adv. Funct. Mater.* **2021,** *31* (28), 2101523.

15. Lin, D.; Liu, Y.; Cui, Y. Reviving the Lithium Metal Anode for High-Energy Batteries. *Nat. Nanotechnol.* **2017,** *12* (3), 194-206.

16. Wu, Y.; Wang, S.; Li, H.; Chen, L.; Wu, F. Progress In Thermal Stability of All-Solid-State-Li-Ion-Batteries. *Info. Mat.* **2021,** *3* (8), 827-853.

17. Li, H. Electrochemical Impedance Spectroscopy Study on Using $Li_{10}GeP_2S_{12}$ Electrolyte for All-Solid-State Lithium Batteries. *Int. J. of Electrochem. Sc.* **2021**, *16*, 210229.

18. Shi, Y.; Zhou, D.; Li, M.; Wang, C.; Wei, W.; Liu, G.; Jiang, M.; Fan, W.; Zhang, Z.; Yao, X. Surface Engineered Li Metal Anode for All-Solid-State Lithium Metal Batteries with High Capacity. *ChemElectroChem* **2021,** *8* (2), 386-389.

19. Shen, L.; Zhao, C.; Weng, W.; Li, M. Q.; Jin, Y.; Zhang, Z. H.; Yao, X. Y. In Situ-Formed LiF-Rich Multifunctional Interfaces toward Stable $Li_{10}GeP_2S_{12}$-Based All-Solid-State Lithium Batteries. *Adv. Mater. Interfaces* **2022,** *9* (24), 2200822.

20. Ma, J.; Quhe, R.; Zhang, Z.; Yang, C.; Zhang, X.; Li, J.; Xu, L.; Yang, J.; Shi, B.; Liu, S.; Xu, L.; Sun, X.; Lu, J. Two-Dimensional Materials as a Stabilized Interphase for the Solid-State Electrolyte $Li_{10}GeP_2S_{12}$ in Lithium Metal Batteries. *J. Mater. Chem. A* **2021,** *9* (8), 4810-4821.

21. Li, M. Q.; Zhou, D.; Wang, C.; Weng, W.; Jiang, M.; Liu, G. Z.; Yao, X. Y.; He, H. In Situ Formed Li-Ag Alloy Interface Enables $Li_{10}GeP_2S_{12}$-Based All-Solid-State Lithium Batteries. *ACS Appl. Mater. Interfaces* **2021,** *13* (42), 50076-50082.

22. Wan, H.; Liu, S.; Deng, T.; Xu, J.; Zhang, J.; He, X.; Ji, X.; Yao, X.; Wang, C. Bifunctional Interphase-Enabled $Li_{10}GeP_2S_{12}$ Electrolytes for Lithium–Sulfur Battery. *ACS Energy Lett.* **2021,** *6* (3), 862-868.

23. Zhang, N.; Lv, Z.-C.; Zhao, Y.-S.; Zhang, J.-H.; Zhu, Y.-R.; Yi, T.-F. Construction of $Na_2Li_2Ti_6O_{14}$@$LiAlO_2$ Composites as Anode Materials of Lithium-Ion Battery with High Performance. *Acta Metall. Sin.* **2022,** *35* (12), 2047-2056.

24. Ma, Y.; Xu, M.; Zhang, J.; Liu, R.; Wang, Y.; Xiao, H.; Huang, Y.; Yuan, G. Improving Electrochemical Performance of Ni-Rich $LiNi_{0.8}Co_{0.1}Mn_{0.1}O_2$ Cathode for Li-ion Batteries by Dual-Conductive Coating Layer of PPy and $LiAlO_2$. *J. Alloy. Compd.* **2020,** *848*, 156387.

25. Wakudkar, P.; Deshpande, A. V., Enhancement of Ionic Conductivity by Addition of $LiAlO_2$ in $Li_{6.6}La_3Zr_{1.6}Sb_{0.4}O_{12}$ for Lithium Ion Battery. *Solid State Ionics* **2020,** *345*, 115185.

26. Yasmeen, S.; Ryu, S. W.; Lee, S. H.; Lee, H. B. R. Atomic Layer Deposition Beyond Thin Film Deposition Technology. *Adv. Mater. Technol.* **2022***,* 2200876.

27. Liu, W.; Liu, D.; Zhang, Y.; Li, B. Numerical Investigation of Particle Size Distribution, Particle Transport and Deposition in a Modified Chemical Vapor Deposition Process. *Powder Technol.* **2022,** *407*, 117616.

28. Li, J.; Ren, G. K.; Chen, J.; Chen, X.; Wu, W.; Liu, Y.; Chen, X.; Song, J.; Lin, Y.

H.; Shi, Y. Facilitating Complex Thin Film Deposition by Using Magnetron Sputtering: A Review. *Jom* **2022,** *74* (8), 3069-3081.

29. Tayyebi, A.; Rastgoo, A.; Osgouie, K. G. The Manufacture and Study of the Microstructure, Mechanical Properties, and Corrosion Behavior of $Fe_{31}Cr_{15}Mo_{14}C_{10}B_{10}Si_5Ti_{15}$ Metallic Glass Thin Film, Prepared by the Magnetic Sputtering Method. *J. Non-Cryst. Solids* **2022,** *595*, 121805.

30. Jiang, M.; Xu, K.; Liao, N.; Zheng, B. Effect of Sputtering Power on Piezoresistivity and Interfacial Strength of SiCN Thin Films Prepared by Magnetic Sputtering. *Ceram. Int.* **2022,** *48* (2), 2112-2117.

31. Lordan, D.; Wei, G.; McCloskey, P.; O'Mathuna, C.; Masood, A. Origin of Perpendicular Magnetic Anisotropy in Amorphous Thin Films. *Sci. Rep.* **2021,** *11* (1), 3734.

32. Wu, Y.; Li, Y. F.; Wang, L. Y.; Bai, Y. J.; Zhao, Z. Y.; Yin, L. W.; Li, H. Enhancing the Li-Ion Storage Performance of Graphite Anode Material Modified by $LiAlO_2$. *Electrochimic Acta* **2017,** *235*, 463-470.

33. Monroe, C.; Newman, J. The Impact of Elastic Deformation on Deposition Kinetics at Lithium/Polymer Interfaces. *J. Electrochem. Soc.* **2005,** *152* (2), A396-A404.

34. Cheng, X. B.; Peng, H. J.; Huang, J. Q.; Wei, F.; Zhang, Q. Dendrite-Free Nanostructured Anode: Entrapment of Lithium in a 3D Fibrous Matrix for Ultra-Stable Lithium-Sulfur Batteries. *Small* **2014,** *10* (21), 4257-63.

35. Ma, Y.; Wang, L.; Fu, S.; Luo, R.; Qu, W.; Hu, X.; Chen, R.; Wu, F.; Li, L. In Situ Formation of a Li–Sn Alloy Protected Layer for Inducing Lateral Growth of Dendrites.

J. Mater. Chem. A **2020,** *8* (44), 23574-23579.

36. Kasemchainan, J.; Zekoll, S.; Spencer Jolly, D.; Ning, Z.; Hartley, G. O.; Marrow, J.; Bruce, P. G. Critical Stripping Current Leads to Dendrite Formation on Plating in Lithium Anode Solid Electrolyte Cells. *Nat. Mater.* **2019,** *18* (10), 1105-1111.

TABLE OF CONTENTS